Chemistry–A European Journal
Research Article
doi.org/10.1002/chem.202303251
Chemistry Europe
European Chemical Societies Publishing
www.chemeurj.org

Hot Paper

Please Mind the Gap: Highly Condensed P–N Networks in LiP_4N_7 and $Li_{3-x}P_6N_{11-x}(NH)_x$

Stefanie Schneider,[a] Sebastian Klenk,[a] Simon D. Kloss,[a] and Wolfgang Schnick*[a]

Alkali nitridophosphates AP_4N_7 and $A_3P_6N_{11}$ (A = Na, K, Rb, Cs) have been known for decades. However, their Li homologues have remained elusive. In this work, the highly condensed lithium (imido)nitridophosphates LiP_4N_7 and $Li_{3-x}P_6N_{11-x}(NH)_x$ (x = 1.66(3)) were synthesized from $LiPN_2$ and P_3N_5 in the multianvil press at 10 GPa. They constitute the first lithium nitridophosphates with 3D networks exhibiting a degree of condensation larger than 0.5 and high thermal stability. LiP_4N_7 crystallizes in the orthorhombic space group $P2_12_12_1$ with a = 4.5846(6) Å, b = 8.0094(11) Å, and c = 13.252(2) Å (Z = 4). $Li_{3-x}P_6N_{11-x}(NH)_x$ crystallizes in the triclinic space group $P\bar{1}$ with Z = 2, a = 4.6911(11) Å, b = 7.024(2) Å, c = 12.736(3) Å, α = 87.726(11), β = 80.279(11), and γ = 70.551(12)°. Both compounds are stable against hydrolysis in air.

Introduction

Although nitridophosphates have been thoroughly investigated over the past 30 years, the limits of this compound class have not yet been reached. Research in this field does not just continuously grow outward, there also remain surprising knowledge gaps to be filled.

One way to visualize where there are gaps in the field, is the degree of condensation κ (Figure 1). κ represents the quotient of the number of central atoms to vertex atoms in a tetrahedral network and was originally developed to describe Si–O networks.[1] Its lower and upper limits are the non-condensed tetrahedron (κ = 0.25) and the value of the binary compound. In the case of silicates this is SiO_2 with κ = 0.5. Since P–N compounds are formed from PN_4-tetrahedra similarly to SiO_4 in silicates, κ can also be used to describe nitridophosphate structures. Due to κ > 0.5 in the upper limit P_3N_5, triply coordinated vertices can be found in nitridophosphates in contrast to silicates.

Comparing silicates and phosphates, some degrees of condensation appear repeatedly. There are several common degrees of condensation that can be observed in nitridophosphates and that occur throughout series of homologs. They are accompanied by structural motifs like non-condensed tetrahedra (κ = 1/4) in Li_7PN_4,[2] rings of three or chains of tetrahedra (κ = 1/3) in $Li_{12}P_3N_9$, Li_4PN_3 or AE_2PN_3 (AE = Mg, Ca),[3,4] adamantane-like supertetrahedra or layers in $Li_{10}P_4N_{10}$, $Li_5P_2N_5$ (κ = 2/5)[5–7] or $RE_2P_3N_7$ (RE = La, Ce, Pr; κ = 3/7).[8] In the range of highly condensed structures ($\kappa \geq$ 0.5), motifs are connected to three-dimensional networks with N connecting two (κ = 1/2) or three (κ = 6/11, 4/7) tetrahedra. This is known from compounds like APN_2 (A = H, Li, Na),[9–13] AEP_2N_4 (AE = Be, Ca, Sr, Ba),[14–17] AP_6N_{11} (A = Na, K, Rb, Cs),[18,19] and AP_4N_7 (A = H, Na, Ka, Rb, Cs).[20–25]

Notably, the two common κ of 6/11 and 4/7 have been described for all alkali metals except for Li. This seems surprising, since Li-containing solids play a major role in today's technologies, mainly as battery materials.[26–29] However, just this seems to have stunted research of highly condensed lithium nitridophosphates, as high conductivity is rather expected in compounds with a high Li content.[3,6,7,30]

Surprisingly, the single publication claiming synthesis of LiP_4N_7 stems from a period in which Li batteries have not played such a large role as yet.[31] In 1985, the compound was obtained as semi-amorphous powder from LiH and PNH_2 in NH_3 gas flow, but the structure could not be elucidated at the time. Theoretical calculations have simulated the structure with models of HP_4N_7 and NaP_4N_7.[32]

In this work, we present the synthesis and structural characterization of LiP_4N_7 and $Li_{3-x}P_6N_{11-x}(NH)_x$. They are the first representatives in the Li–P–N system with κ > 0.5, closing the obvious gaps in the series AP_4N_7 (A = H, Na, K, Rb, Cs), and $A_3P_6N_{11}$ (A = Na, K, Rb, Cs) phases.

Results and Discussion

Synthesis

LiP_4N_7 and $Li_{3-x}P_6N_{11-x}(NH)_x$ were obtained upon reaction of $LiPN_2$ and P_3N_5 at 10 GPa and 1150 °C, using a multianvil press with a modified Walker-type module. Single crystals were obtained of both phases. Optimization of synthesis procedures showed short reaction durations to promote formation of LiP_4N_7, whereas longer duration promotes formation of

[a] S. Schneider, S. Klenk, S. D. Kloss, Prof. Dr. W. Schnick
Department of Chemistry
University of Munich (LMU)
Butenandtstraße 5–13 (D), 81377 Munich (Germany)
E-mail: wolfgang.schnick@uni-muenchen.de

Supporting information for this article is available on the WWW under https://doi.org/10.1002/chem.202303251

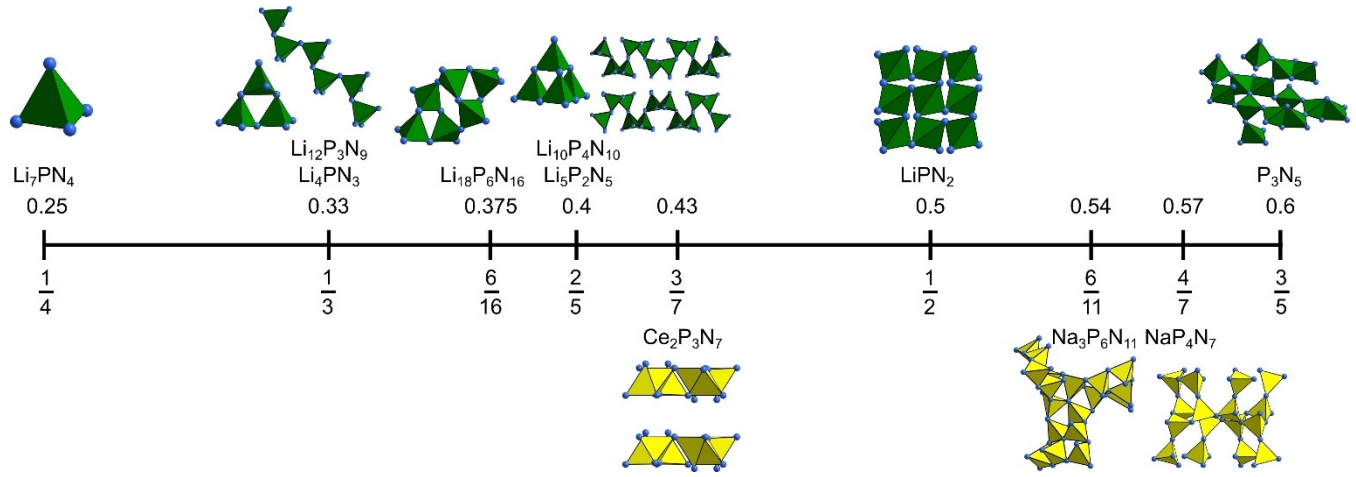

Figure 1. Visualization of the degree of condensation κ. Shown are the structural motifs of Li_7PN_4,[2] $Li_{12}P_3N_9$,[3] Li_3PN_4,[3] $Li_{10}P_4N_{10}$,[5] $Li_5P_2N_5$,[7] $Ce_2P_3N_7$,[8] $LiPN_2$,[12] $Na_3P_6N_{11}$,[25] NaP_4N_7,[23] and P_3N_5[33] with their respective degrees of condensation κ. At $\kappa < 0.5$, motifs of several tetrahedra or layers occur, at $\kappa \geq 0.5$, 3D networks are observed. Lithium oxonitridophosphates are shown in green, other nitridophosphates in yellow.

$Li_{3-x}P_6N_{11-x}(NH)_x$. Due to the close similarity in reaction conditions, no phase pure product could be obtained. Syntheses of these phases is very sensitive against small changes in reaction parameters and do not follow idealized reaction Equations (1) and (2).

$$P_3N_5 + LiPN_2 \rightarrow LiP_4N_7 \quad (1)$$

$$P_3N_5 + 3\ LiPN_2 \rightarrow Li_3P_6N_{11} \quad (2)$$

LiP_4N_7 was obtained as main phase from stoichiometric use of starting materials. However, formation of $LiPN_2$ and $Li_{3-x}P_6N_{11-x}(NH)_x$ side phases could not be omitted.

Instead of formation of $Li_3P_6N_{11}$, H was incorporated into the structure. Possibly, the H source was superficially hydrolyzed crucible material *h*BN. Stoichiometric use of starting materials according to equation (2) in a dried *h*BN crucible did not yield $Li_{3-x}P_6N_{11-x}(NH)_x$, but $LiPN_2$ and LiP_4N_7. Formation of $LiPN_2$ and LiP_4N_7 side phases could not be omitted.

Possibly, use of different precursors might enable more different reaction conditions following other synthesis strategies for nitrides like the azide route[19,23] or lithium nitride self-flux.[3,6,7,30] For example, HPN_2 could be used for targeted introduction of H.

Samples with the highest phase content of LiP_4N_7 and $Li_{3-x}P_6N_{11-x}(NH)_x$ were used for Rietveld refinement (Figures 2, S1, S2, Table S8), to corroborate the structural models as obtained from single-crystal X-ray diffraction data.

Crystal Structure

The crystal structures of LiP_4N_7 and $Li_{3-x}P_6N_{11-x}(NH)_x$ were determined by single-crystal X-ray diffraction (scXRD). The structures were solved using direct methods and Li positions were determined by difference Fourier synthesis.

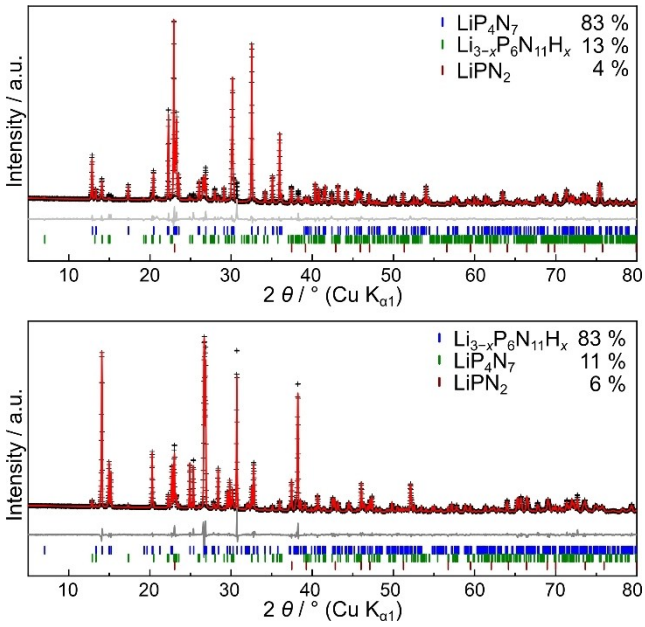

Figure 2. Rietveld refinement of the samples with highest content of LiP_4N_7 (top) and $Li_{3-x}P_6N_{11-x}(NH)_x$ (bottom). Measured with Cu $K_{\alpha1}$ radiation. Measured intensities are shown with black crosses, calculated and residual intensities are shown as red and gray lines, respectively. Possible reflection positions are shown with markers according to the legends in the graphs.

LiP_4N_7: LiP_4N_7 crystallizes in the orthorhombic space group $P2_12_12_1$ (no. 19) with $a = 4.5846(6)$, $b = 8.0094(11)$, $c = 13.252(2)$ Å, and $Z = 4$. Additional crystallographic data are listed in Table 1. The structure consists of four P positions that are tetrahedrally coordinated by N. All seven N positions connect at least two tetrahedra, with two N positions, N3 and N6, connecting three tetrahedra (Figure 3a). The sole Li position is embedded into this network (Figure 3e).

The network can be most easily explained by following the connectivity of N3 and N6, the two N positions connecting three tetrahedra to propeller-like motifs similar to those in β-

Table 1. Crystallographic details on the refinement from single crystal data of LiP_4N_7 and $Li_{3-x}P_6N_{11-x}(NH)_x$.

Sum formula	LiP_4N_7	$Li_{1.34}P_6N_{9.34}(NH)_{1.66}$
Formula weight/g·mol^{-1}	228.89	350.90
Crystal system	Orthorhombic	Triclinic
Space group	$P2_12_12_1$ (no. 19)	$P\bar{1}$ (no. 2)
Lattice parameters/Å, °	$a=4.5823(9)$ $b=8.0066(9)$ $c=13.2407(18)$	$a=4.6911(11)$ $b=7.024(2)$ $c=12.736(3)$ $\alpha=87.726(11)$ $\beta=80.279(11)$ $\gamma=70.551(12)$
Cell volume/Å^3	485.78(13)	390.0(2)
Formula units per unit cell Z	4	2
Density/g·cm^{-3}	3.130	2.988
μ/mm^{-1}	1.465	1.374
Crystal size/mm^3	0.04×0.015×0.015	0.03×0.03×0.02
Radiation (λ/Å)	Mo K_α $\lambda=0.71073$ Å	
Temperature/K	113(2)	111(2)
θ-range/°	$2.973\leq\theta\leq31.518$	$3.1\leq\theta\leq32.0$
Total no. of reflections	6132	7400
Independent reflections	1626	2693
Refined parameters	109	169
R_{int}; R_σ	0.0375; 0.0364	0.0428; 0.0558
$R1$ (all data); $R1$ ($F^2>2\sigma(F^2)$)	0.0302; 0.0271	0.0602; 0.0410
$wR2$ (all data); $wR2$ ($F^2>2\sigma(F^2)$)	0.0650; 0.0642	0.0989; 0.0932
Goodness of fit (χ^2)	1.159	1.028
$\Delta\rho_{max}$; $\Delta\rho_{min}$/e·Å^{-3}	0.494; −0.406	0.695; −1.097

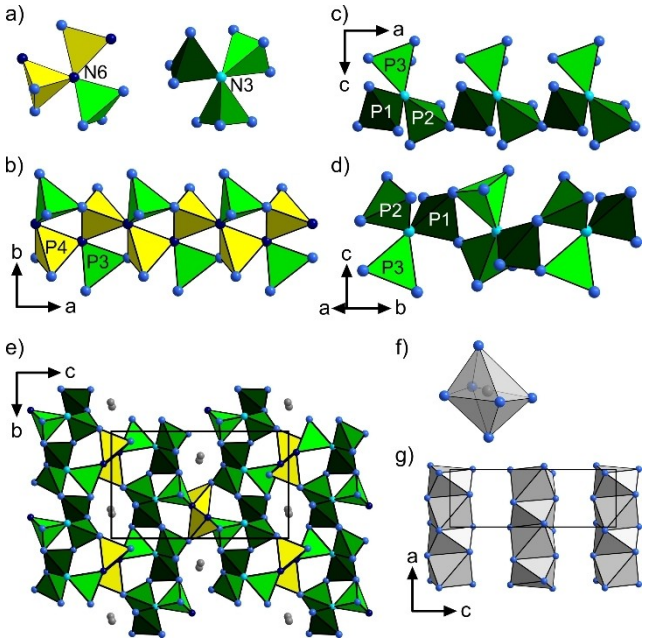

Figure 3. Network structure of LiP_4N_7. a) Triply coordinated N6 (dark blue, left) and N3 (light blue, right). b) Connectivity of P4 tetrahedra (yellow) around N6 (dark blue). c) Connectivity of P1, P2, and P3 tetrahedra (dark green, green and bright green, respectively) around N3 (light blue) along [100]. d) Connectivity of P1, P2, and P3 bands along [010]. e) Network structure of LiP_4N_7 in and around the unit cell. Li cations are shown in gray. f) Coordination polyhedron around Li. g) Columns of LiN_6 octahedra along [100].

HP_4N_7. N6 connects two instances of P4 tetrahedra and one additional P3 tetrahedron (Figure 3a). N6 occurs as two vertices of the P4 tetrahedron, resulting in a P4–N6–P4–N6 backbone with one P3 tetrahedron connected to each N6. These P3 tetrahedra share another vertex with one P4 tetrahedron. This leads to bands of propeller-like motifs that share both P4 tetrahedra and are additionally connected by one vertex. The resulting *dreier*-rings (*Liebau* nomenclature) are connected along [100] (Figure 3b).[1]

N3 connects P1, P2, and P3 tetrahedra. This triplet shares the N4 vertex with symmetrically identical tetrahedra along [100] (Figure 3c). These bands of triplets are in turn connected along [010] by N1 and N7 of the P1 tetrahedron, forming further *dreier*-rings (Figure 3d) and resulting in layers of triplets around N3 in the (001) plane. Along [001], these layers are connected by the tetrahedra around P4–N6–P4–N6 backbone (Figure 3e). The network has the hitherto unknown topological point symbol $\{3^2.4.5^3.6^4\}\{3^2.4^2.5^2.6^4\}\{3^4.4^3.5^4.6^4\}\{3^4.4^4.5^5.6^2\}$, which was calculated using ToposPro.[34]

The single crystallographic Li position has a distorted octahedral coordination sphere which shares two opposite faces with symmetrically identical LiN_6-octahedra, forming strands along [100] (see Figure 3f + g). Possibly, Li is slightly mobile, both within the large coordination polyhedron, and along strands of face-sharing LiN_6 octahedra. This could explain its large displacement (0.129(9) Å^2). In principle, it is possible that instead of full occupancy of Li, H or O is incorporated into the structure. However, difference Fourier analysis did not show residual electron density at suitable distances to N to support presence of H. Furthermore, since no phase pure sample could be obtained, bulk methods like Fourier-transform infrared (FTIR) spectroscopy or nuclear magnetic resonance (NMR) spectroscopy cannot unequivocally prove presence of H. Thus, we have chosen to use the stoichiometric notation LiP_4N_7.

$Li_{3-x}P_6N_{11-x}(NH)_x$: $Li_{3-x}P_6N_{11-x}(NH)_x$ crystallizes in the triclinic space group $P\bar{1}$ (no. 2) with $a=4.6911(11)$, $b=7.024(2)$, $c=12.736(3)$ Å, $\alpha=87.726(11)$, $\beta=80.279(11)$, $\gamma=70.551(12)$°, and $Z=2$. Crystallographic details are listed in Table 1. As in LiP_4N_7, vertex-sharing PN_4-tetrahedra constitute the 3D-network. All N atoms connect at least two tetrahedra, with N1 and N7 connecting three tetrahedra.

There are two crystallographically different propeller-like motifs, comparable to those in $BaP_6N_{10}NH$ (Figure 4a).[35] N1 is coordinated by three P atoms: P1, P2, and P3. This triplet of tetrahedra is connected to crystallographically identical motifs, forming bands of *dreier*-rings along [100] (Figure 4b). These bands are stacked along [010], connected by P2 and P3 tetrahedra. This leads to *vierer*-rings of P2 and P3 tetrahedra, with P1 tetrahedra protruding along [100] (Figure 4c). P1 and P3 form *vierer*-rings again, connecting these stacks to layers in

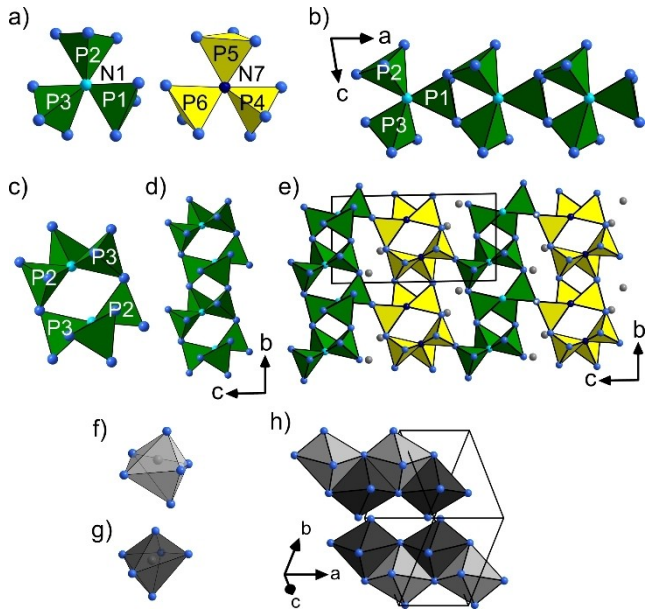

Figure 4. Structure of $Li_{3-x}P_6N_{11-x}(NH)_x$. a) Propeller-like motifs around N1 (light blue, green tetrahedra, left) and N7 (dark blue, yellow tetrahedra, right). b) Propeller-like structure motifs are connected along [100] via two N (blue). c) Bands of propeller-motifs are connected to stacks with P1 tetrahedra protruding to each side, forming *vierer*-rings along [010]. d) Connection of stacks along [010] forming layers in the (001) plane. e) Layers of crystallographically different propeller motifs are connected along [001]. f) Distorted LiN_6 octahedron around Li1. g) Distorted LiN_6 octahedron around Li2. h) Edge-sharing LiN_6 octahedra connected along [100].

the a,b-plane. The layers are connected along [001] to crystallographically different layers with the same constitution to form a three-dimensional network with large gaps containing Li-ions and H (Figure 4d). The point symbol for the net is $\{3^2.4^2.5^2.6^2.7.8\}\{3^2.4^2.5^2.6^4\}\{3^2.4^4.5^3.7\}$ and was calculated using ToposPro.[34] No network with this point symbol has been reported as yet.

Li positions were determined using difference Fourier synthesis and imply full and partial occupancy of Li1 and Li2, respectively. The distorted LiN_6 octahedra are connected by edges along [100] (Figure 4e–g). Possibly, more than one H per formula unit can be inserted in the structure, which is also corroborated by the presence of several resonances visible in NMR spectra. Since the position of H could not be determined unequivocally, its positions were constrained onto a singly bridging N atom with the largest possible distance to Li (N5) and an N position with remaining electron density at an appropriate distance to N (N4). The occupancy of the latter H position was constrained to partial occupancy of the Li2 position. With full and partial occupancies for H1 and H2, respectively, scXRD suggests an H content of $x = 1.66(3)$. However, for quantitative analysis of H content in the bulk, phase-pure samples are necessary. Thus, the notation indicating a phase-width was chosen: $Li_{3-x}P_6N_{11-x}(NH)_x$.

In other $AE_3P_6N_{11}$ (AE = Na, K), boiling in concentrated acids was found to replace metal positions with oxonium ions. Heating of the compounds with metal chlorides can replace ions, since cations are only coordinated weakly.[24] A similar mechanism could be conceivable for $Li_{3-x}P_6N_{11-x}(NH)_x$. Furthermore, by ion exchange, it might be possible to synthesize other highly condensed networks like a $Li_3P_6N_{11}$ phase with the structure type and network topology of $Na_3P_6N_{11}$ or $K_3P_6N_{11}$ or vice versa.

Nuclear Magnetic Resonance and Fourier-Transform Infrared Spectroscopy

Due to the low electron density of hydrogen, its presence in the structure cannot be confirmed unequivocally by XRD methods. Therefore, nuclear magnetic resonance (NMR) and Fourier-transform infrared (FTIR) spectroscopy were employed. However, since no phase pure samples were available, the informative value of these investigations has to be considered carefully.

^{31}P, coupled $^{31}P\{^1H\}$ and ^7Li NMR spectra of two samples with LiP_4N_7 and $Li_{3-x}P_6N_{11-x}(NH)_x$ as main P-containing phases were measured (Figures S7–S12). However, due to unavailability of phase pure samples, assignment of signals to crystallographic positions is not possible.

^{31}P NMR spectra were compared in order to assign the resonances to the respective phases (Figure S13a). ^{31}P resonances of LiP_4N_7 occur at −8.4 and −15.9 ppm, those of $Li_{3-x}P_6N_{11-x}(NH)_x$ at 0.8 and −3.0 ppm. Possibly, the signal at −15.9 ppm contains portions of both LiP_4N_7 and $Li_{3-x}P_6N_{11-x}(NH)_x$.

The $^{31}P\{^1H\}$ coupled spectrum shows presence of H in the sample with $Li_{3-x}P_6N_{11-x}(NH)_x$ as main P-containing phase (Figure S11). However, no quantitative information can be derived from the spectrum. In the $^{31}P\{^1H\}$ coupled spectrum of a sample consisting mainly of LiP_4N_7, there are also smaller signals. However, since the side phase contains H, its presence cannot be confirmed or excluded definitely.

^7Li spectra each show a single signal at −0.3 and −0.2 ppm. These signals are very similar and in the range of other chemical shifts for ^7Li.[3,6,7,30]

The FTIR spectrum of a sample consisting mainly of LiP_4N_7 (69% LiP_4N_7, 19% $Li_{3-x}P_6N_{11-x}(NH)_x$, 12% $LiPN_2$) shows no significant absorption bands in the area around 2500–3500 cm^{-1}, in which N–H or O–H absorption bands would be expected (Figure 5, black line). The small signal at 3340 cm^{-1} can be explained by 19% of H-containing side phase $Li_{3-x}P_6N_{11-x}(NH)_x$ or superficial hydrolysis, indicating that no significant amount of H is present in the sample. Increased noise in the area from 2400–1900 cm^{-1} is due to C–C bonds in the diamond window of the ATR unit. The spectrum shows three mayor groups of absorption bands, which is in accordance with literature.[31] However, comparison to literature is difficult, both because the IR spectrum from literature has low resolution and because no phase pure samples could be obtained.

The P–N vibration modes in the fingerprint area of $Li_{3-x}P_6N_{11-x}(NH)_x$ are very similar to those of LiP_4N_7 (Figure 5, gray line). However, absorption of N–H vibrational modes is visible at 3220 cm^{-1}, corroborating the presence of H.

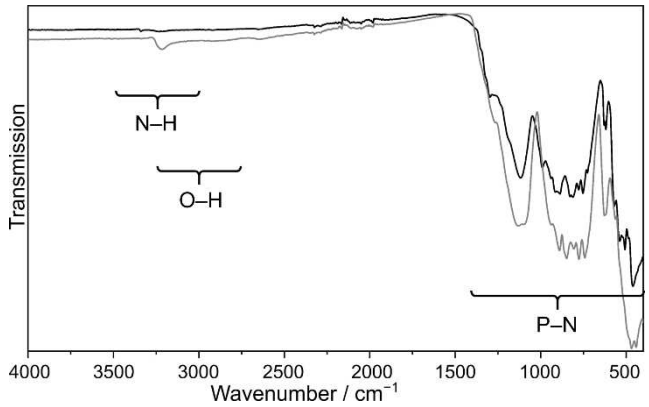

Figure 5. FTIR spectrum of a sample with LiP_4N_7 as main phase (69% LiP_4N_7, 19% $Li_{3-x}P_6N_{11-x}(NH)_x$, 12% $LiPN_2$, black line), and $Li_{3-x}P_6N_{11-x}(NH)_x$ (83% $Li_{3-x}P_6N_{11-x}(NH)_x$, 11% LiP_4N_7, 6% $LiPN_2$, gray line). The spectrum was measured under Ar atmosphere with an ATR unit with a diamond window. Increased background in the area around 1900–2300 cm^{-1} results from C–C vibrations in the diamond window.

Thermal Stability

The thermal stability of LiP_4N_7 and $Li_{3-x}P_6N_{11-x}(NH)_x$ was investigated using variable-temperature XRD. For LiP_4N_7, no decomposition was observed up to 900 °C, solely a small thermal shift of lattice parameters is visible. Above 900 °C, additional reflections of low intensity appear that could not be assigned to known phases (Figure 6a). Thermal expansion coefficients were calculated using lattice parameters from Rietveld refinement at temperatures from room temperature up to 1000 °C. The expansion of the *a* and *b* lattice parameters is very similar with $\alpha_a = 4.42(5)\times10^{-6}$ and $4.4(2)\times10^{-6}$ K^{-1}. This might be a result of the high connectivity along [100] and [010]. Along [001], the structure is more open, which is reflected in the larger thermal expansion along this direction ($\alpha_c = 8.5(2)\times10^{-6}$ K^{-1}). The volumetric expansion coefficient $\alpha_V = 17.5(4)\times10^{-6}$ K^{-1} (Figure 6c), is in a range comparable to other nitridophosphates with $\kappa = 4/7$.[36]

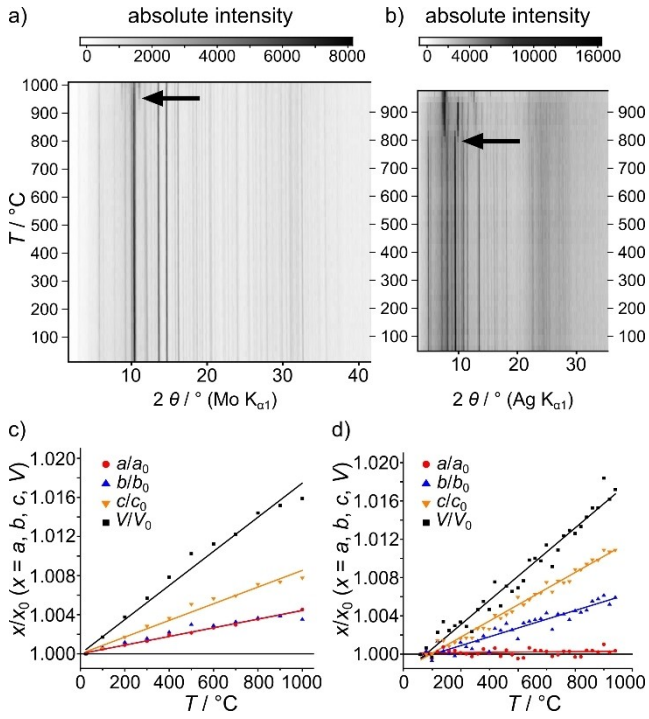

Figure 6. Thermal stability measurements and thermal expansion. a) Variable temperature powder X-ray diffractograms of LiP_4N_7 measured from 40–1000 °C with Mo $K_{\alpha1}$ radiation. An arrow marks beginning decomposition. b) Variable temperature powder X-ray diffractogram of $Li_{3-x}P_6N_{11-x}(NH)_x$ measured from 60–900 °C with Ag $K_{\alpha1}$ radiation. An arrow marks beginning decomposition.

At 800 °C, incipient decomposition of $Li_{3-x}P_6N_{11-x}(NH)_x$ is observed. Only Li_3P is visible in the diffraction pattern at 840 °C and above (Figure 6b). Li_3P can often be observed in lithium nitridophosphate syntheses at high temperatures and is a common decomposition product.[6,7]

The thermal expansion coefficient was calculated as described above (Figure 6d). Thermal expansion along [100] could not be reliably determined in the temperature range available ($\alpha_a = 0.2(3)\times10^{-6}$ K^{-1}). This might be due to the highly condensed *dreier*-rings along [100] that cannot be stretched as much as the more open features along [010] and [001]. Expansion along [010] and [001] are $9.2(5)\times10^{-6}$ and $16.9(4)\times10^{-6}$ K^{-1}, respectively. The volumetric expansion coefficient of $\alpha_V = 25.2(8)\times10^{-6}$ K^{-1} is comparable to other nitridophosphates with $\kappa = 6/11$ like $BaP_6N_{10}NH$ ($\alpha_V = 22.2\times10^{-6}$ K^{-1}),[35] $Rb_3P_6N_{11}$ ($\alpha_V = 13.9\times10^{-6}$ K^{-1}),[19] or $Cs_3P_6N_{11}$ ($\alpha_V = 13.0\times10^{-6}$ K^{-1}).[19] The error margin in $Li_{3-x}P_6N_{11-x}(NH)_x$ is higher and deviation of values larger than in LiP_4N_7, since the determination of lattice parameters with Ag $K_{\alpha1}$ is less exact than with Mo $K_{\alpha1}$.

The high degree of condensation accounts for the high stability of the compounds. Both LiP_4N_7 and $Li_{3-x}P_6N_{11-x}(NH)_x$ are stable against hydrolysis and can be stored under ambient conditions indefinitely.

This is consistent with the general correlation of stability and the degree of condensation that can be found in other nitridophosphates and silicates. Whereas Li_7PN_4 is highly sensitive against air and moisture and can only be handled in inert conditions,[2] $Li_{10}P_4N_{10}$ can be washed with dry ethanol[6] and $LiPN_2$ is stable against acids and bases.[10] LiP_4N_7 and $Li_{3-x}P_6N_{11-x}(NH)_x$ were washed with concentrated acids without indication of decomposition.

Conclusions

The two highly condensed lithium (imido)nitridophosphates LiP_4N_7 and $Li_{3-x}P_6N_{11-x}(NH)_x$ were synthesized and characterized. Their structures were solved and refined from scXRD data. The high degree of condensation is realized by N atoms triply coordinated by P. In LiP_4N_7, one of these N atom positions occurs twice in one tetrahedron, resulting in a band of propeller-like motifs similar to those in β-HP_4N_7, sharing tetrahedra. The resulting highly condensed band of *dreier*-rings is connected to additional propeller-like motifs. $Li_{3-x}P_6N_{11-x}(NH)_x$ exhibits two triply by P coordinated N atom positions. Here, both form propeller-like motifs, which share corners to other

propeller motifs. For more information on the H position in $Li_{3-x}P_6N_{11-x}(NH)_x$, neutron powder diffraction would be a helpful tool.

In comparison to other lithium nitridophosphates, both compounds show high thermal and chemical stability, which is likely due to their highly condensed network structure. Both compounds are stable against hydrolysis and can be stored at ambient conditions indefinitely. The degree of condensation is also expressed in the relatively low thermal expansion coefficient.

In further research, the questions of H content and positions, ionic conductivity, and potential synthesis at milder conditions will be addressed. Synthesis of these compounds fills the gap of nitridophosphates with the formula type AP_4N_7 (*A*=H, Na, K, Rb, Cs) and $A_3P_6N_{11}$ (*A*=Na, K, Rb, Cs).

Experimental Section

Synthesis of P_3N_5: P_4S_{10} (Sigma Aldrich, 99%) was saturated with NH_3 for 4 h in a dried silica tube. Then it was heated to 1125 K at 5 Kmin^{-1} in an NH_3 gas flow for 4 h following the procedure described by Stock et al.[37] The resulting powder was washed with water, ethanol, and acetone and dried under vacuum. Phase purity was confirmed by powder XRD, FTIR and CHNS combustion analysis.

Synthesis of $LiPN_2$: P_3N_5 and Li_3N (Rockwood Lithium, 94%) in a molar ratio of 1:1.2 were ground in an agate mortar under inert atmosphere in an Ar-filled glovebox (Unilab, MBraun, Garching, $O_2 < 1$ ppm, $H_2O < 0.1$ ppm) and transferred to a Ta crucible within a silica tube in Ar atmosphere. The sealed silica tube was heated to 800 °C. The product was washed with diluted hydrochloric acid, water, and ethanol, and dried under vacuum.

High-pressure synthesis of LiP_4N_7 and $Li_{3-x}P_6N_{11-x}(NH)_x$: For high-pressure synthesis, a modified Walker-type multianvil press was used.[38,39] P_3N_5 and $LiPN_2$ were ground in a 1:1 ratio (1:3 for $Li_{3-x}P_6N_{11-x}(NH)_x$) and packed in a hexagonal boron nitride crucible (Henze, Kempten), which was closed with a *h*BN lid. The crucible was placed in the center of an MgO octahedron (doped with 5% Cr_2O_3, edge length 18 mm, Ceramic Substrates & Components Ltd, Isle of Wight) using MgO spacers (Cesima Ceramics, Wust-Fischbach). Resistance heating using two graphite furnaces (Schunk Kohlenstofftechnik GmbH, Zolling) that were contacted to the anvils of the multianvil press by Mo discs ensured heating of the sample. A ZrO_2 tube (Cesima Ceramics, Wust-Fischbach) provided thermal insulation. The octahedron was placed between WC cubes (doped with 7% Co, Hawedia, Marklkofen, Germany) with truncated edges (edge length 11 mm), and separated with pyrophillite gaskets (Ceramic Substrates & Components, Isle of Wight, UK). Additional details about the multianvil press and its experimental setup is given in literature.[39]

The samples were first compressed to 10 GPa. For LiP_4N_7, the samples were then heated to 1150 °C over a period of 30 min, held for 15 min and cooled down over a period of 30 min. For $Li_{3-x}P_6N_{11-x}(NH)_x$, the temperature was raised to 1150 °C over 60 min, held for 60 min, and cooled down over 60 min. Eventually, the pressure was slowly decreased. The resulting gray product was isolated and washed with water.

Single crystal X-ray diffraction: A D8 Venture diffractometer (Bruker, Billerica MA, USA) was used with Mo K_α radiation from a rotating anode source to obtain scXRD data. Data was corrected for absorption with SADABS and integrated using the APEX3 program package.[40,41] ShelXT was used to solve the structure and ShelXL was used for refinement.[42] P and N atoms, as well as one Li position in $Li_{3-x}P_6N_{11-x}(NH)_x$ were refined anisotropically. Li positions were found by difference fourier synthesis. Diamond3 was used for crystal structure visualization.[43]

Deposition Number(s) CSD2290091 and CSD2290093 contain(s) the supplementary crystallographic data for this paper. These data are provided free of charge by the joint Cambridge Crystallographic Data Centre and Fachinformationszentrum Karlsruhe Access Structures service.

Powder X-ray diffraction: The powder was sealed into a glass capillary (Ø = 0.5 mm, wall thickness 0.1 mm, Hilgenberg GmbH). A Stoe STADI P diffractometer (Stoe & Cie, Darmstadt, Germany) with Cu $K_{\alpha1}$ radiation ($\lambda = 1.5406$ Å), Ge(111) monochromator and a Mythen 1 K detector (Dectris, Baden, Switzerland) in parafocusing Debye–Scherrer geometry was used to analyze the sample. The TOPAS 6 program package was used for Rietveld refinements.[44]

Variable-temperature XRD was performed on a Stoe STADI P diffractometer (Stoe & Cie, Darmstadt, Germany) with Mo $K_{\alpha1}$ radiation ($\lambda = 0.71073$ Å, for $Li_{3-x}P_6N_{11-x}(NH)_x$ Ag $K_{\alpha1}$ radiation, $\lambda = 0.5594075$ Å). The diffractometer is equipped with a Ge(111) monochromator. A IP PDS plate detector was used for data acquisition. Rietveld refinement was performed with the TOPAS 6 program package.[44]

Solid-state magic angle spinning (MAS) nuclear magnetic resonance (NMR) spectroscopy: ^{31}P, coupled $^{31}P\{^1H\}$, and ^7Li spectra were measured using a DSX Avance spectrometer (Bruker) with a magnetic field of 11.7 T. The rotors containing the samples (Ø = 2.5 mm) were spun with a rotation frequency of 20 kHz on a commercial MAS probe (Bruker). Topspin (Bruker) was used for analyzation of the spectra.[45]

Fourier-transform Infrared (FTIR) Spectroscopy: Measurement of FTIR spectra was performed on a Bruker FTIR Alpha II compact spectrometer with diamond ATR unit in Ar atmosphere. Data was obtained from 400–4000 cm^{-1} using the OPUS program package.[46]

Elemental analyses: Due to the presence of side phases in all samples, elemental analysis is difficult in the case of LiP_4N_7 and $Li_{3-x}P_6N_{11-x}(NH)_x$. Furthermore, Li, P, N, and H cannot be observed simultaneously with a single method. Li and H cannot be observed in energy-dispersive X-ray (EDX) spectroscopy, CHNS cannot measure P or Li. Thus, even the combination of methods offers only vague results. Thus, elemental analysis was only used to confirm that no additional elements are present in the samples.

Energy-dispersive X-ray spectroscopy (EDX): A scanning electron microscope (SEM) JSM-6500F (Jeol, Tokyo, Japan; maximum acceleration voltage 30 kV) was used to examine a carbon-coated sample. An energy dispersive spectrometer (Model 7418, Oxford Instruments, Abingdon, United Kingdom) was used for qualitative and semiquantitative elemental analysis. The obtained data was analyzed with INCA.[47]

Mass spectrometry (CHNS): CHNS spectrometry data was acquired using a Vario MICRO Cube device (Elementar, Langenselbold, Germany).

Supporting Information

The authors have cited additional references within the Supporting Information.[3,6,7,30]

Acknowledgements

The authors thank Dr. Lisa Gamperl, Christian Minke (both at Department of Chemistry of LMU), and Armin Schulz (MPI FKF Stuttgart) for SEM/EDX, NMR, and Raman measurements, respectively. Funding support from the Deutsche Forschungsgemeinschaft (DFG, German Research Foundation) under Germany's Excellence Strategy–EXC 2089/1-390776260 (e-Conversion) is gratefully acknowledged. Open Access funding enabled and organized by Projekt DEAL.

Conflict of Interests

The authors declare no conflict of interest.

Data Availability Statement

The data that support the findings of this study are available in the supplementary material of this article.

Keywords: high-pressure chemistry · lithium · nitridophosphates · solid-state structures

[1] F. Liebau, *Structural Chemistry of Silicates*, Springer, Berlin Heidelberg, **1985**.
[2] W. Schnick, J. Luecke, *J. Solid State Chem.* **1990**, *87*, 101–106.
[3] E.-M. Bertschler, R. Niklaus, W. Schnick, *Chem. Eur. J.* **2017**, *23*, 9592–9599.
[4] V. Schultz-Coulon, W. Schnick, *Z. Anorg. Allg. Chem.* **1997**, *623*, 69–74.
[5] W. Schnick, U. Berger, *Angew. Chem. Int. Ed.* **1991**, *30*, 830–831; *Angew. Chem.* **1991**, *103*, 857–858.
[6] E.-M. Bertschler, C. Dietrich, T. Leichtweiß, J. Janek, W. Schnick, *Chem. Eur. J.* **2018**, *24*, 196–205.
[7] E.-M. Bertschler, R. Niklaus, W. Schnick, *Chem. Eur. J.* **2018**, *24*, 736–742.
[8] S. D. Kloß, N. Weidmann, R. Niklaus, W. Schnick, *Inorg. Chem.* **2016**, *55*, 9400–9409.
[9] H. Jacobs, R. Nymwegen, S. Doyle, T. Wroblewski, W. Kockelmann, *Z. Anorg. Allg. Chem.* **1997**, *623*, 1467–1474.
[10] P. Eckerlin, C. Langereis, I. Maak, A. Rabenau, *Angew. Chem.* **1960**, *7*, 19561.
[11] R. Marchand, P. L'Haridon, Y. Laurent, *J. Solid State Chem.* **1982**, *43*, 126–130.
[12] W. Schnick, J. Lücke, *Z. Anorg. Allg. Chem.* **1990**, *588*, 19–25.
[13] K. Landskron, S. Schmid, W. Schnick, *Z. Anorg. Allg. Chem.* **2001**, *627*, 2469–2472.
[14] F. J. Pucher, S. Rebecca Römer, F. W. Karau, W. G. Schnick, *Chem. Eur. J.* **2010**, *16*, 7208–7214.
[15] F. J. Pucher, A. Marchuk, P. J. Schmidt, D. Wiechert, W. Schnick, *Chem. Eur. J.* **2015**, *21*, 6443–6448.
[16] F. W. Karau, L. Seyfarth, O. Oeckler, J. Senker, K. Landskron, W. Schnick, *Chem. Eur. J.* **2007**, *13*, 6841–6852.
[17] F. W. Karau, W. Schnick, *J. Solid State Chem.* **2005**, *178*, 135–141.
[18] H. Jacobs, R. Nymwegen, *Z. Anorg. Allg. Chem.* **1997**, *623*, 429–433.
[19] K. Landskron, W. Schnick, *J. Solid State Chem.* **2001**, *156*, 390–393.
[20] S. Horstmann, E. Irran, W. Schnick, *Angew. Chem. Int. Ed.* **1997**, *36*, 1992–1994; *Angew. Chem.* **1997**, *109*, 2085–2087.
[21] D. Baumann, W. Schnick, *Inorg. Chem.* **2014**, *53*, 7977–7982.
[22] D. Baumann, W. Schnick, *Angew. Chem. Int. Ed.* **2014**, *53*, 14490–14493; *Angew. Chem.* **2014**, *126*, 14718–14721.
[23] K. Landskron, E. Irran, W. Schnick, *Chem. Eur. J.* **1999**, *5*, 2548–2553.
[24] A. A. Vitola, J. Ronis, T. Millers, *Izv. Akad. Nauk Latv. SSR Seriya Khimicheskaya* **1990**, *1*, 35–39.
[25] J. Ronis, B. Bondars, A. A. Vitola, T. Millers, *Latv. PSR Zinat. Akad. Kim. Serija1* **1990**, *3*, 299–301.
[26] M. Park, X. Zhang, M. Chung, G. B. Less, A. M. Sastry, *J. Power Sources* **2010**, *195*, 7904–7929.
[27] T. H. Kim, J. S. Park, S. K. Chang, S. Choi, J. H. Ryu, H. K. Song, *Adv. Energy Mater.* **2012**, *2*, 860–872.
[28] N. Boaretto, I. Garbayo, S. Valiyaveettil-SobhanRaj, A. Quintela, C. Li, M. Casas-Cabanas, F. Aguesse, *J. Power Sources* **2021**, *502*, 1–34.
[29] J. Li, J. Fleetwood, W. B. Hawley, W. Kays, *Chem. Rev.* **2022**, *122*, 903–956.
[30] E.-M. Bertschler, C. Dietrich, J. Janek, W. Schnick, *Chem. Eur. J.* **2017**, *23*, 2185–2191.
[31] A. Vitola, V. Avotins, I. Lange, G. Smilškalne, T. Millers, *Latv. J. Chem.* **1985**, *3*, 288–292.
[32] Y. A. Du, N. A. W. Holzwarth, *Phys. Rev. B* **2010**, *81*, 1–15.
[33] S. Horstmann, E. Irran, W. Schnick, *Z. Anorg. Allg. Chem.* **1998**, *624*, 620–628.
[34] V. A. Blatov, A. P. Shevchenko, *Topos Pro v. 5.1.5.7*, TOPOS Expert **n.d**.
[35] S. Wendl, L. Eisenburger, M. Zipkat, D. Günther, J. P. Wright, P. J. Schmidt, O. Oeckler, W. Schnick, *Chem. Eur. J.* **2020**, *26*, 5010–5016.
[36] S. Wendl, L. Eisenburger, P. Strobel, D. Günther, J. P. Wright, P. J. Schmidt, O. Oeckler, W. Schnick, *Chem. Eur. J.* **2020**, *26*, 7292–7298.
[37] A. Stock, B. Hoffmann, *Ber. Dtsch. Chem. Ges.* **1903**, *36*, 314–319.
[38] D. Walker, *Am. Mineral.* **1991**, *76*, 1092–1100.
[39] H. Huppertz, *Z. Kristallogr.* **2004**, *219*, 330–338.
[40] Bruker, *SADABS*, Bruker AXS Inc., Madison, WI, USA **2009**.
[41] Bruker, *APEX3 V2018.1-0* **2018**.
[42] G. M. Sheldrick, *Acta Crystallogr. Sect. C* **2015**, *71*, 3–8.
[43] K. Brandenburg, *Diamond Version 3.2k*, Crystal Impact GbR, Bonn, Germany **2014**.
[44] A. A. Coelho, *TOPAS Academic Version 6*, Coelho Software, Brisbane, Australia **2016**.
[45] Bruker, *Topspin v.3.0 Pl 3*, Bruker Biospin GmbH, Germany **2010**.
[46] Bruker, *OPUS Version 8.7*, Bruker Optik GmbH, Ettlingen, Germany **2021**.
[47] *INCA Version 4.02*, Oxford Instruments, Analytical Limited, Abingdon, United Kingdom **n.d**.

Manuscript received: October 4, 2023
Accepted manuscript online: October 24, 2023
Version of record online: November 20, 2023